Journal of the European Ceramic Society **15** (1995) 297–305

0955-2219/95/$9.50

Toughening of X-Sialon with Al_2O_3 Platelets

Y. Zhou, J. Vleugels, T. Laoui & O. Van der Biest

Department of Metallurgy and Materials Engineering, Katholieke Universiteit Leuven, De Croylaan 2, B-3001 Leuven, Belgium

(Received 28 January 1994; revised version received 15 July 1994; accepted 11 August 1994)

Abstract

Toughening of an X-sialon matrix with up to 53 volume percent Al_2O_3 platelets was investigated. The effect of platelet content on both matrix phase composition and mechanical properties of the composites was evaluated. The extent of cracks introduced by Vickers hardness indentations showed a reduced length with increasing platelet content, indicating an increase in fracture toughness. The toughness has been shown to increase from 1·77 MPa · $m^{1/2}$ for pure X-sialon up to 4·16 MPa · $m^{1/2}$ for the composite containing 28 volume percent platelets. For higher platelet additions, toughness increases further but the composition of the matrix shifts to β'-sialon. The E*-modulus of the composites increases with the amount of platelets. The improvement in fracture toughness was attributed to debonding, crack bridging and crack deflection.*

1 Introduction

Sialon ceramics have been investigated extensively due to their remarkable properties which make them suitable for high temperature structural applications.[1–3] They are also being considered for cutting tools; β'-sialons for instance are already being used for machining of cast irons, but they are not suitable for most steels. Our recent research has shown that at the high cutting speeds at which ceramic cutting tools need to be used to be competitive, chemical compatibility with the workpiece material may be a more important selection criterion than other material properties such as hardness.[4,5] A recent study showed that X-sialon ceramics exhibit a much better chemical compatibility with steel at high temperatures compared to β'-sialon based ceramics.[6] The high chemical wear resistance of X-sialon may indicate that cutting tools could be an interesting potential application. However, actual turning trials[7] indicated that the poor toughness of the material caused frequent chipping of the cutting edge. An indentation fracture toughness value of about 1·77 MPa $m^{1/2}$ was measured.[6] The low fracture toughness of X-sialon will thus limit the use of this ceramic in the field of cutting tools.

To overcome this common problem encountered in the application of monolithic ceramic materials, many attempts have been made to improve their fracture toughness. For instance, the incorporation of a second phase into the monolithic ceramic matrix can result in an improved fracture toughness of the composite. Toughening of ceramics has usually focused on the introduction of whiskers into the matrix phase. A recent concern regarding the reinforcing components has shown less interest in whiskers because of several unfavourable aspects, including the high price, toxicity and difficulty in achieving a uniform dispersion during processing. Platelets could be a good alternative to whiskers as a reinforcement in monolithic ceramics because the toughening mechanisms contributing to whisker composites such as crack bridging, debonding, pullout and crack deflection could also operate in platelet ceramic composites.[8,9] Furthermore, the use of platelets in ceramic composites has some advantages over whisker reinforced ceramics, including the ease of dispersion into ceramic matrix at high loading without agglomerates, safer handling and lower cost. In this study, Al_2O_3 platelets are selected to toughen X-sialon ceramic matrix. According to the Si–Al–O–N phase diagram[1] both matrix and reinforcement should be in chemical equilibrium.

A limited number of studies have been published concerning platelet reinforced ceramics. To our knowledge, toughening of X-sialon with Al_2O_3 platelets has never been reported in the literature. In a Si_3N_4–SiC platelet system, Hanninen reported that there was a dependence of fracture toughness on platelet content and direction.[10] A maximum value of 9·9 MPa · $m^{1/2}$ was obtained at 25 vol.% platelets in the plane parallel to the hot press axis and perpendicular to the platelet basal faces, whereas a toughness of 6·8 MPa · $m^{1/2}$ was obtained for the unreinforced Si_3N_4 matrix.[10] Claussen achieved a toughness of 8 MPa · $m^{1/2}$ from approximately 4·8 MPa · $m^{1/2}$ for the matrix, in RBSN with 20 vol.% SiC platelets.[9] In both cases toughness was enhanced, but strength dropped with the

Table 1. Characteristics of starting materials given by the supplier

Si_3N_4	N:	38·36 wt%	FSSS*:	0·41 μm
grade HCST	C:	0·15 wt%	BET:	19·1 m^2/g
LC12-SX	O:	2·06 wt%	β-Si_3N_4:	97%
Starck Berlin	Fe:	70 ppm		
	Al:	46 ppm		
	Ca:	12 ppm		
Al_2O_3	Na:	40 ppm	Particle	
grade SM8	Fe:	15 ppm	size:	submicron
Bailkowski	Si:	60 ppm	α-Al_2O_3:	95%
	Ca:	10 ppm		
	K:	60 ppm		
	Others:	<5 ppm		
SiO_2	Purity:	99·8%		
fumed	Particle			
Sigma U.S.A.	size:	0·014 μm		
Al_2O_3 Platelet	Al:	51%		
grade 2	O:	47%		
Atochem France	F:	1–2%		
	Na:	1500 ppm		
	Si:	500 ppm		
	S:	250 ppm		
	Ca:	200 ppm		
	Size:	10–15 μm diameter		
		1 μm thickness		

*Mean particle size as determined by using Fisher Subsieve Sizer.

addition of platelets into a Si_3N_4 matrix. Ketchion *et al.* attempted to improve the properties of a Si_3N_4 matrix by adding SiC whiskers and platelets.[11] Their results showed that there was no drastic increase in the fracture toughness, nevertheless the platelet containing composites had slightly better values than those containing whiskers. On the other hand, strength was reported to be maintained in the whisker reinforced samples, while there was a significant drop in those containing platelets. Literature on Al_2O_3–SiC platelet composites has also shown an increase in toughness and a decrease in strength with respect to the matrix. For instance, Fischer *et al.* have reported that the toughness of the Al_2O_3-SiC platelet composite increased from the base value for alumina of 4·35 to 5·68 MPa · $m^{1/2}$ for a 30 vol.% SiC platelet loaded sample, while the strength decreased from 346·1 to 198·4 MPa.[12] Becher reported fracture toughness values for SiC platelet reinforced Al_2O_3 close to those obtained with whiskers.[13] As to Al_2O_3 platelet reinforced ceramic composites, Claussen has reported, in a study on a TZP – Al_2O_3 platelet system, an increase in toughness in a low toughness TZP matrix with increasing platelet addition, but a decrease in toughness in a high toughness TZP matrix.[9] The strength dependence was reversed, i.e. the low toughness TZP matrix showed a decrease in strength with increasing platelet content.

Fig. 1. SEM micrograph of Al_2O_3 platelets.

The objective of this study is to investigate the possibility of X-sialon matrix composites reinforced with Al_2O_3-platelets in various volume fractions. Composites with Al_2O_3 platelet loading up to 53 vol.% were fabricated. Their microstructure and mechanical properties were evaluated and compared to the unreinforced X-sialon matrix material.

2 Experimental Procedure

The composition of the composites was based on $Si_{12}Al_{18}O_{39}N_8$ as a matrix material with a wide range of Al_2O_3 platelet addition. The starting materials used in this study were Si_3N_4, Al_2O_3, SiO_2 powders and Al_2O_3 platelet. Their characteristics are summarised in Table 1. The morphology of Al_2O_3 platelets is shown in Fig. 1.

The powder–platelet mixtures were processed via a wet mixing technique. The Al_2O_3 platelet and Si_3N_4, SiO_2 and Al_2O_3 powders in a desired composition were mixed with ethanol, using high density alumina cylinders as media, for about 72 h.

The resulting slurries were then heated on a sand bath for about 1–2 days in order to evaporate the alcohol. The mixture of platelet–powders obtained after drying was in the form of granulates.

A dense product was obtained by hot-pressing using graphite dies under moderate vacuum (<1 Pa). Hot-pressing schedule followed in this study is the same as the one reported in previous work,[6] e.g. hot-pressing for 1 h at a temperature of 1650°C and a pressure of 30 MPa.

The density of the hot-pressed samples was measured using the water displacement method, recording the mass in air and then immersed in water.

Phase analysis was mainly based on X-ray diffraction patterns obtained either from the hot-pressed surface as received or from a cross-sectioned surface of the specimen. Spectra were recorded using CuKα radiation from 5 to 80° 2θ

at the scan rate of 0·02°/s. Aside from XRD, electron probe micro-analysis (EPMA) was used to assist with phase identification.

The microstructure of the hot-pressed materials and crack propagation from indentation were observed with the scanning electron microscope (JEOL 733). SEM specimens were coated with gold to reduce specimen charging under the electron beam. Secondary and backscattered electron images were recorded at an accelerating voltage of 20 kV.

Vickers hardness was measured on polished samples, using a load of 10 kg. Elastic modulus was measured by the resonance frequency method with a Grindo-sonic apparatus using a test bar of approximately 25 mm long, 4 mm wide and 2·5 mm thick.

Comparative values for the fracture toughness of the different materials were obtained by the indentation method. Examination of crack morphology was made with electron micrographs on Vickers indentations for all specimens. The fracture toughness was calculated using the following equation derived by Anstis *et al.*[14]

$$K_{Ic} = 0{\cdot}016\ (E/Hv)^{1/2}\ P/c^{3/2} \qquad (1)$$

where E is the elastic modulus (Pa); H_v is the Vickers hardness (N/m^2); P is the Vickers load (N); and c is the radius of the crack length (m).

Samples for transmission electron microscope (TEM) were prepared by mechanical thinning, dimpling and then ion milling with an argon beam. Ion milled foils were coated with carbon for the examination in a JEOL 200CX microscope operating at 200 kV.

3 Results

The different grades with the amount of platelets added, are listed in Table 2.

Typical SEM micrographs of the platelet reinforced composites are shown in Figs 2 and 3. The examination of SEM micrographs revealed a dense, crack free hot-pressed body for all the composites. The pores appearing on polished surfaces could be due in part to platelet pullout during polishing. The reinforcing platelets are uniformly dispersed throughout the X-sialon matrix, without apparent cluster formation. However, the platelets are anisotropically oriented, with their basal planes preferentially aligned normal to the hot-pressing direction. This type of orientation of platelets suggests that a considerable rearrangement of platelets occurred during the liquid phase sintering of the powder mixture. The alignment of platelets was facilitated by the uni-axial load during hot pressing.

Table 2. Platelet content of the composite materials and phases identified by XRD

Sample	*Volume percent of platelets (vol. %)*	*Phase type*		
		X-sialon	*β'-sialon*	*α-Alumina*
XA0	0	X-sialon		
XA7	7·179	X-sialon		Al_2O_3
XA13	13·39	X-sialon		Al_2O_3
XA18	18·83	X-sialon		Al_2O_3
XA23	23·63	X-sialon		Al_2O_3
XA28	27·88	X-sialon		Al_2O_3
XA43	43·61	X-sialon	β'-sialon	Al_2O_3
XA53	53·71		β'-sialon	Al_2O_3

When the volume fraction of Al_2O_3 platelets increased to 53%, platelets appeared more interlocked and locally sintered together, the microstructure obtained was free of cracks and large pores as shown in Fig. 3.

The results of the X-ray diffraction (XRD) phase analysis of the hot pressed composites are summarised in Table 2. A single X-sialon phase pattern was found in sample XA0, corresponding to an Al_2O_3-platelet free X-sialon starting composition. Both X-sialon and Al_2O_3, which are the main and secondary phases, respectively, were observed in

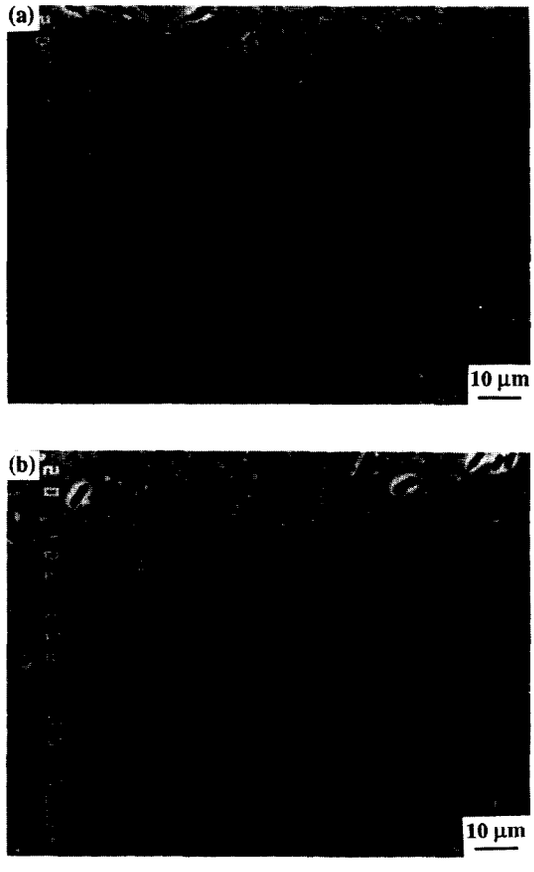

Fig. 2. SEM micrographs of the polished sections of Al_2O_3-platelet–X-sialon matrix composite containing 28 vol.% platelets. (a) Normal to the hot-pressing direction. (b) Parallel to the hot-pressing direction.

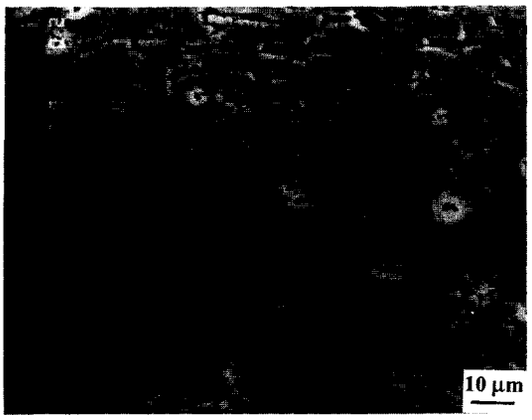

Fig. 3. SEM micrographs of the polished cross-section of sample XA53 containing 53 vol.% of the platelets.

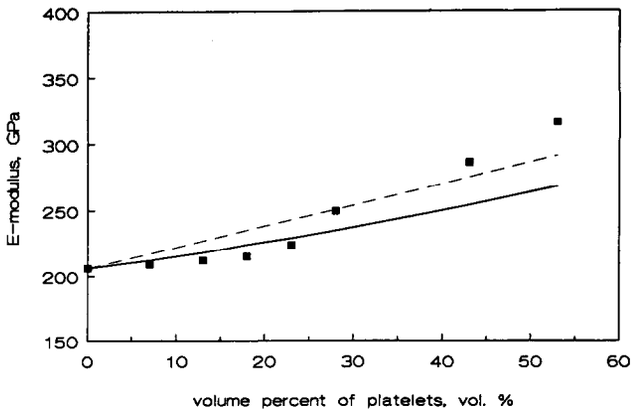

Fig. 4. E-modules vs Al_2O_3 platelet content. Calculated curves according to formula (2) and (3) are indicated.

all X-sialon composite samples with a platelet content up to 28 vol.%. If the platelet content is further increased, β'-sialon is formed in addition to X-sialon. In the composite grade XA53, containing 53 vol.% platelets, the matrix phase is β'-sialon and no X-sialon could be detected.

The measured and calculated densities of the hot-pressed sialon–Al_2O_3 platelet composites are listed in Table 3. The pure X-sialon was found to be pore-free by ceramography and was assumed to be 100% dense. The value of 3·04 g/cm^3 corresponds well with the value of 3·00 g/cm^3 reported by Zangvil *et al.*[15] The calculated density in Table 3 was estimated from nominal volume fraction of intended X-sialon matrix and reinforcing Al_2O_3 platelet, taking the constituent phase density of pure X-sialon phase as 3·04 g/cm^3 and that of Al_2O_3 as 3·93 g/cm^3.

The measured elastic modulus as a function of Al_2O_3 platelet content is shown in Fig. 4. An E-modulus of 367 GPa for a pure dense Al_2O_3 sample processed under the same experimental condition was obtained by Grindo-sonic measurement, thus slightly lower than 380 GPa given as a typical value for dense alumina.[16] The E-modulus obtained in all Al_2O_3 platelet reinforced sialon

Table 3. Measured and calculated densities and Vickers hardness (HV) of sialon–Al_2O_3 composites. The Vickers hardness was measured on a cross-section parallel to the hot-press axis, for directions perpendicular (PER) and parallel (PAR) to the hot-press axis

Sample	*Density g/cm³ (measured)*	*Density g/cm³ (calculated)*	*Percent of calculated value*	*Hardness kg/mm²*	
				$Hv10^{PER}$	$Hv10^{PAR}$
XA0	3·04			1256	1278
XA7	3·09	3·10	99·68	1304	1278
XA13	3·11	3·16	98·42	1288	1220
XA18	3·14	3·21	97·82	1272	1241
XA23	3·16	3·25	97·23	1208	1220
XA28	3·18	3·29	96·66	1270	1222
XA43	3·59	3·43	104·6	1490	1382
XA53	3·76	3·52	106·8	1306	1227

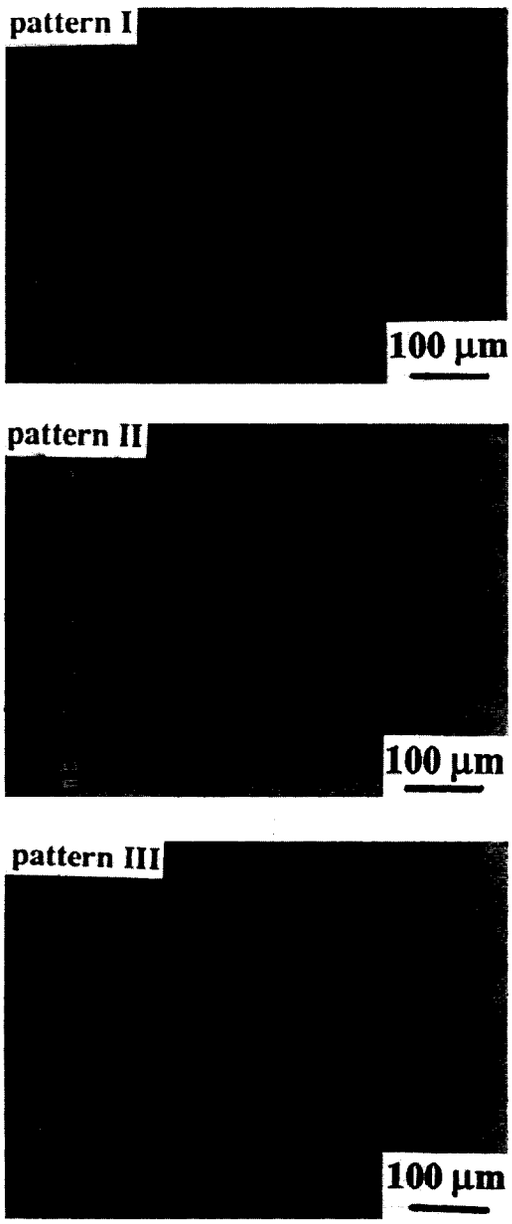

Fig. 5. Illustration of three types of indentation crack patterns. Pattern I: chipping as main feature (pure X-phase sample). Pattern II: well developed crack traces (platelet volume fraction lower than 28%), Pattern III: disruption of clearly defined cracks (platelet volume fraction higher than 28%). The hot-pressing direction is vertically oriented.

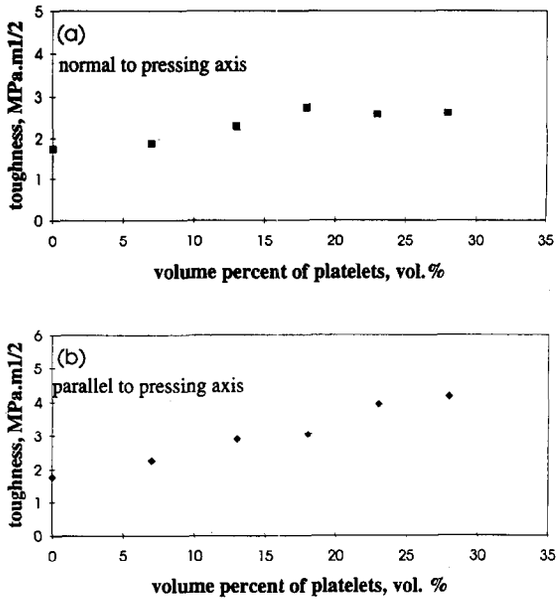

Fig. 6. Fracture toughness as a function of platelet volume fraction in two directions; (a) normal to pressing direction, and (b) parallel to pressing direction.

composites has shown an increase with respect to the platelets content.

The hardness values determined for each sample from Vickers indentation are the average data of five tests. A 10 kg load was applied on a polished cross-section parallel to the hot-press axis, taking care to align the diagonals of the impression with one normal to the hot-pressing axis and the other parallel to the hot-pressing axis in order to identify if there is any anisotropy in hardness. Indentation measurements indicated essentially similar hardness levels between 1200 and 1300 kg/mm^2 for all composite samples, except for the one with 43 vol.% platelets which showed approximately an increase in hardness by 18%, compared to an unreinforced X-sialon matrix (Table 3).

Figure 5 shows three types of indentation crack patterns observed around Vickers hardness indents. The main feature of crack pattern I is chipping around indentation. The pure X-phase sample XA0 was almost exclusively matching pattern I and measurement of crack length was difficult. The brittle nature of X-sialon is evidently illustrated by crack pattern I. Crack pattern II gives clearly defined radial cracks and the crack length was easily measured. Most reinforced X-sialon composites, e.g. XA7, XA13, XA18, XA23, XA28, showed this crack pattern, indicating an improved toughness relative to X-sialon. Crack pattern III shows multiple cracking with cracks emanating from corners as well as from the sides of the indent and is accordingly unsuitable for crack size measurement. Samples XA43 and XA53 have this type of disrupted crack pattern.

Figure 6 shows the fracture toughness of the reinforced composites as a function of direction

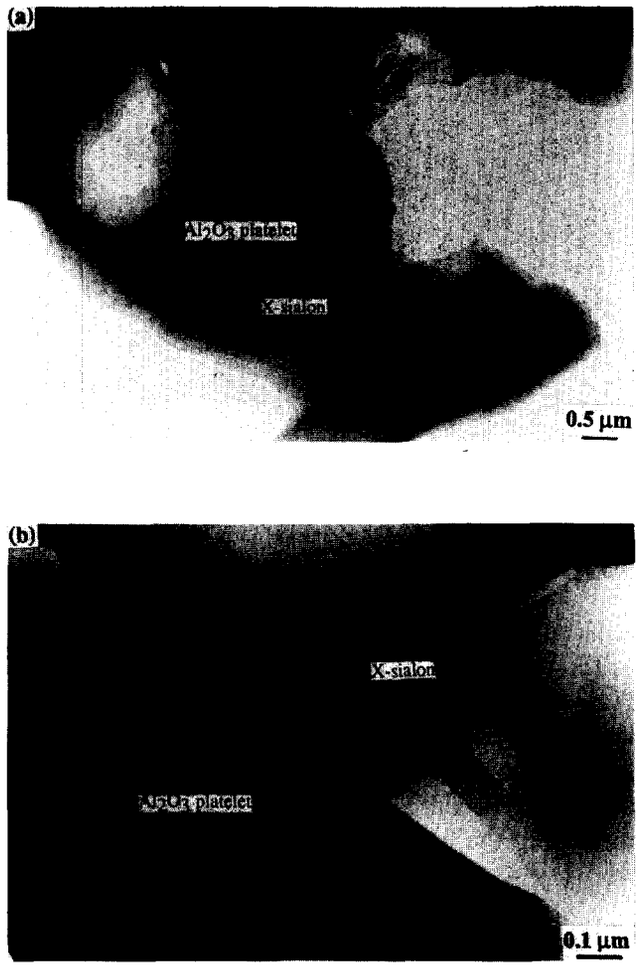

Fig. 7. TEM micrographs (a) and (b) of X-sialon matrix composite with 28 vol.% Al_2O_3 platelets showing a clean interface between X-sialon matrix and Al_2O_3 platelets.

and Al_2O_3 platelet content. There was a general increase in the fracture toughness with increasing platelet content both normal and parallel to the hot-pressing direction. However, a great deal of difference in K_{Ic} values obtained in both directions was noticeable.

For X-sialon based composites, the highest K_{Ic} value was 4·16 MPa · m$^{1/2}$ for a 28 vol.% Al_2O_3 platelet containing sample, whereas unreinforced X-sialon was only 1·77 MPa · m$^{1/2}$. When the addition of platelets exceeded 28 vol.% the value of fracture toughness could not be precisely evaluated with a Vickers indentation method due to disruption of a well defined crack propagation pattern. However, visual examination of these cracks shown in Fig. 5 reveals an apparent shortening of crack length both parallel and normal to the hot-pressing direction for higher platelet loaded sialon composites, indicating that the crack resistance is considerably enhanced. A toughness of about 7 MPa · m$^{1/2}$ could be estimated from the extent of the diagonal cracks parallel to the hot-pressing direction for a composite with nominally 53 vol.% platelets.

In TEM micrographs (Fig. 7) a clean interface between the smoothly contoured platelet and the

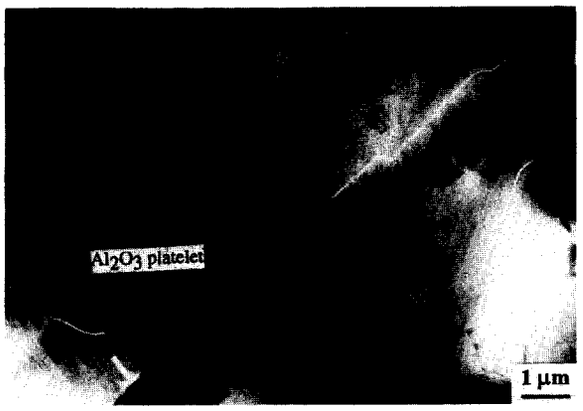

Fig. 8. TEM micrograph of X-sialon matrix composite with 28 vol.% Al_2O_3 platelets showing a crack following the X-sialon matrix–Al_2O_3 platelets interface. The arrow marks the point where the crack is deflected into the interface. Further along the interface, this crack is not always seen edge-on.

adjacent twinned X-sialon grain is observed down to the resolution at which the sample was examined. However, the existence of a very thin amorphous layer between Al_2O_3 platelets and the surrounding matrix is not excluded. As shown in Fig. 8, debonding occurs along the platelet–matrix interface indicating the weak nature of the interface.

4 Discussion

All specimens were easily fabricated to reach densities of more than 97% theoretical values by uniaxial hot-pressing. Difficulties usually experienced with processing of whisker reinforced ceramic composites such as whisker dispersion and low densities,[17] were essentially avoided. The Al_2O_3 platelets were easily dispersed into the matrix, forming highly densified X-sialon and β'-sialon composites at the hot-pressing temperature and pressure.

Analysis of densities of a series of hot-pressed products were consistent with phase analysis results as shown in Table 2. The theoretical density of Al_2O_3-platelet–X-sialon matrix composites was almost reached in samples containing up to 28 vol.% platelets, whereas the fact that measured densities of composites containing 43 and 53 vol.% platelets were higher than those predicted for the Al_2O_3-platelet–X-sialon composite can be explained by the shift from X-sialon to β'-sialon phase (density is about 3·1–3·2 g/cm^3) and the apparent growth of the platelets.

Indeed if one studies the microstructure of the composite with 53 vol.% platelets (Fig. 3) one notices that the volume fraction of platelets is much higher than the nominal value of 53 vol.%. Also the average size of the platelets appears to have increased somewhat. The composition of the

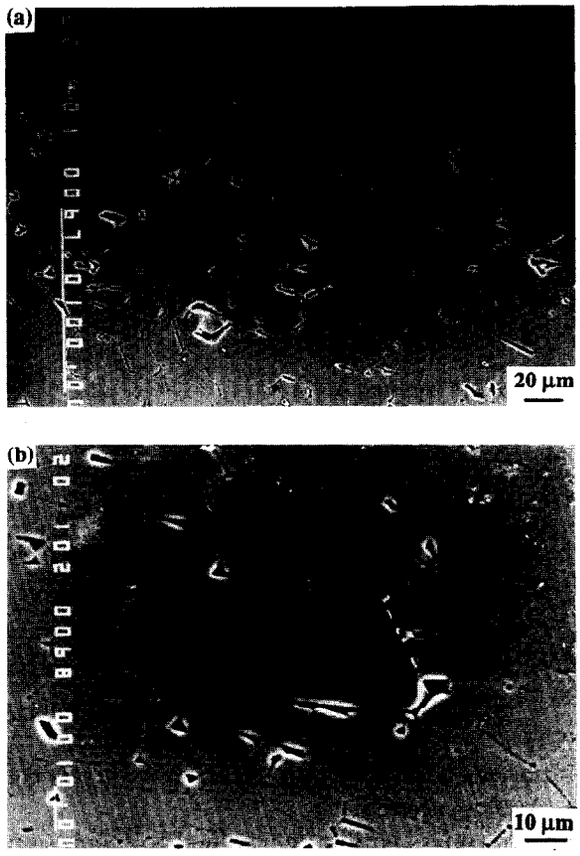

Fig. 9. SEM micrographs of the polished and etched cross section of sample with 53 vol.% Al_2O_3 platelets in Al_2O_3 matrix at two magnification; lower magnification (a) and higher magnification (b).

matrix phase of composite XA53 and pure X-sialon XA0 was compared using EPMA. An average value of 1·28 for Al–Si ratio was obtained in the pure X-sialon sample (XA0), but an average value of 0·72 was obtained in the matrix of a composite with 53 vol.% content of platelets (XA53), indicating a much lower Al content in the matrix composition. Hence it is considered that part of the Al_2O_3 powder which was intended to go to the X-sialon matrix is consumed by the growing platelets. As a consequence, the composition is shifted from the X-sialon composition towards the β'-sialon solubility region in the phase diagram.

To understand the platelet growth at high platelet volume fraction, a composite made with pure Al_2O_3 matrix containing 53 vol.% Al_2O_3 platelets was prepared under the same experimental condition as X-sialon composites. Figure 9 shows the microstructures of this sample which was polished and then etched using HF. Substantial platelet growth was clearly observed in the Al_2O_3 matrix composite with the size of the platelets increasing by a factor of about 6. The equation of the form $G^3-G_0^3 = Kt$,, where G_0 is the initial grain size, G the grain size after hot pressing, t the holding time, and K a temperature-dependent growth rate constant, has been used to

Table 4. Comparison of Al_2O_3 grain growth rate constants

Source	*k* ($\times 10^{-18}$ m^3/s)		
	1600°C	*1650°C*	*1800°C*
Al_2O_3 platelet (in this study):			
parallel to hot-pressing direction		2·24	
perpendicular to hot-pressing direction		146·68	
Pure Al_2O_3 (in Ref. 18)	0·517		
(in Ref. 19)	0·0516		
(in Ref. 20)			980

estimate platelet growth rate and allow direct comparison with Al_2O_3 grain growth rate from the literature.[18–20] The average value of G is equal to $1{\cdot}5L$, where L was the average length of 10 growing platelets in SEM micrographs of the polished cross section. Table 4 shows the results of K obtained both in this study and in the literature. Two points can be noted: first, the platelet growth rate is higher in the direction perpendicular to hot-pressing than the one parallel to hot-pressing. Second, the platelet growth rate perpendicular to the hot-pressing direction is considerably higher than growth rate reported either by Bennison *et al.*[18] or Rödel *et al.*[19] for pure Al_2O_3 at 1600°C, and close to the growth rate reported by Kaysser *et al.*[20] for pure Al_2O_3 at 1800°C. This unusually fast grain growth compared with pure alumina is attributed to the high impurity content of the platelets which includes F, Si, Na and Ca. The observation that platelet growth was much slower in the composite with the same platelet content but with a nominal X-sialon composition, indicates that the presence of silicon nitride appears to slow down the growth of the platelets. It is interesting to note here that β'-sialon can suppress grain growth of alumina.[21] At the lower volume fractions of platelets (28 vol.% and below) no platelet growth was observed. The reasons for that are presumably the higher viscosity of the melt due to the lower impurity content and higher N_2 in the composite composition which may inhibit and suppress growth of Al_2O_3 platelets.

Additional evidence that impurities are responsible for platelet growth can be derived from the following experiments: no shift of matrix composition was found when X-sialon containing 43 and 53 vol.% Al_2O_3 particles (5·5 μm, low soda alumina, grade CTB 3, 99·8%, ALCOA) was processed under the same conditions as the X-sialon–platelet composites. X-sialon matrix was formed in both samples and no β'-sialon could be detected from XRD analysis. Thus the high impurity content of the platelets which includes F, Si, Na and Ca is considered as the main reason for the shift of the matrix composition from the X-sialon into the β'-sialon.

To estimate the E-modulus of Al_2O_3-platelet–X–sialon composites, the formula given by Davidge[22] was applied here, e.g.:

$$E_{\perp HP} = E_1V_1 + E_2V_2 \tag{2}$$

$$E_{\parallel HP} = E_1E_2/(E_2V_1 + E_1V_2) \tag{3}$$

where $E_{\perp HP}$ and $E_{\parallel HP}$ are the E-modulus of the composites in the direction perpendicular and parallel to hot press, corresponding to the direction parallel and normal to the platelet basal plane respectively; E_1 and E_2 represent the E-modulus of matrix phase and reinforcing phase, taking the value of 206 GPa from Grindo-sonic measurement for the pure dense X-sialon and 367 GPa for Al_2O_3; V_1 and V_2 are the nominal volume fractions of the two phases.

As Young's modulus for alumina (367 GPa) is much higher than the one for X-sialon (206 GPa), it is expected that E-modulus of Al_2O_3-platelet–X-sialon composites will increase with increasing platelet volume fraction according to formula (2) or (3). The calculated curves are also indicated in Fig. 4 for comparison with experimental data. Note that the elastic modulus was measured on bars with the long direction normal to the hot-press direction and that these bars were loaded in flexure for the measurement of resonance frequencies. One would expect that for perfect alignment of the platelets formula (2) is applicable rather than formula (3), which indeed is the case for the composite with 28 vol.% platelets, where the platelets are well aligned. At lower volume fractions the data appear to follow formula (3) better. In these composites the alignment with respect to the hot-pressing axis is not perfect. Also the presence of some residual porosity and spontaneous microcracking would need to be taken into account and could explain why the experimental values are slightly below the line for formula (3). In other particulate reinforced composites such as SiC-platelet–Si_3N_4 composite, SiC-platelet–Al_2O_3 composite and some other materials, a decrease of the E-modulus with respect to the matrix has been reported[12,23,24] and has also been attributed to the presence of pores and spontaneous microcracking. In view of the relative magnitude of the thermal expansion coefficient of the two phases ($8{\cdot}0 \times 10^{-6}$/°C for Al_2O_3[16] and $3{\cdot}7$–$4{\cdot}5 \times 10^{-6}$/°C for X-sialon[25]) spontaneous microcracking is also possible here depending on the size of the platelets. The higher values obtained for composites with 43 and 53 vol.% are due to the platelet growth and the change in matrix to β'-sialon which has a higher E-modulus of about 240 GPa.[26]

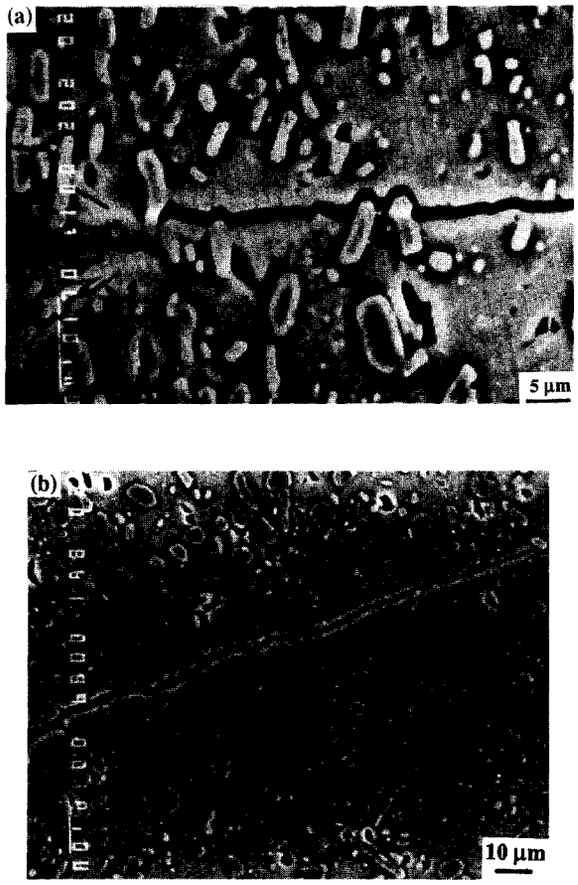

Fig. 10. SEM images of crack propagation in the composite sample with 28 vol.% Al_2O_3 platelets (XA28). (a) Plane parallel to hot-pressing direction. (b) Plane normal to hot-pressing direction.

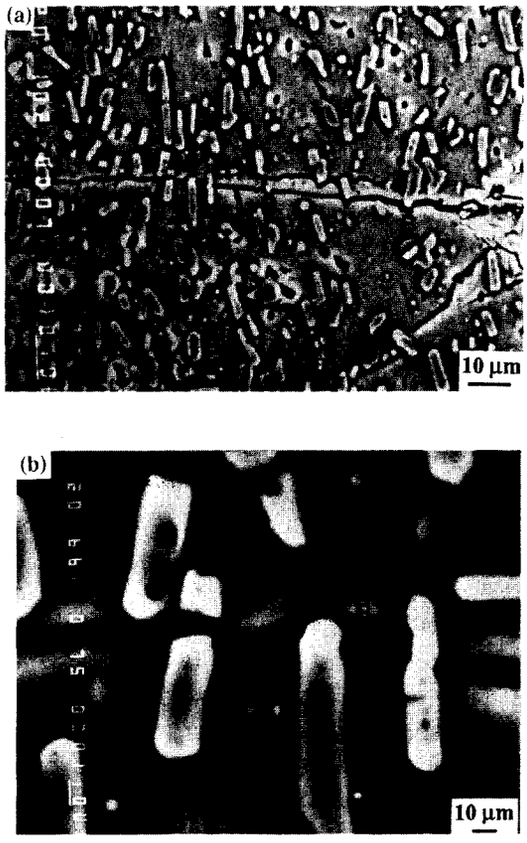

Fig. 11. SEM micrographs (a) and (b) showing crack bridging by Al_2O_3 platelets. B marks bridging sites.

The observed increase in fracture toughness for the Al_2O_3-platelet–sialon matrix composites can be attributed to a combination of crack deflection, crack debonding and crack bridging mechanisms. Figures 10 and 11 further illustrate the extent of crack–microstructure interactions. As shown in Fig. 10, cracks are frequently deflected along platelet–matrix interfaces. In Fig. 11, platelets are seen bridging across the crack wake plane, probably contributing to the greatest extent to the toughness increase over the monolithic X-sialon. A higher degree of toughening was measured when the crack plane propagated parallel to the hot-pressing direction perpendicular to Al_2O_3 platelet basal planes. The increase of fracture toughness increase normal to the hot-pressing axis was lower, because the orientation of platelets is not so favourable for crack deflection and crack bridging.

The composites displayed a much rougher fracture surface as compared to monolithic X-sialon. The fracture surface shown in Fig. 12 (a) illustrates platelet debonding and/or pullout, in contrast to the intragranular fracture exhibited by the unreinforced X-sialon as shown in Fig. 12 (b).

Thermal expansion mismatch and interfacial bonding strength between reinforcing phase and

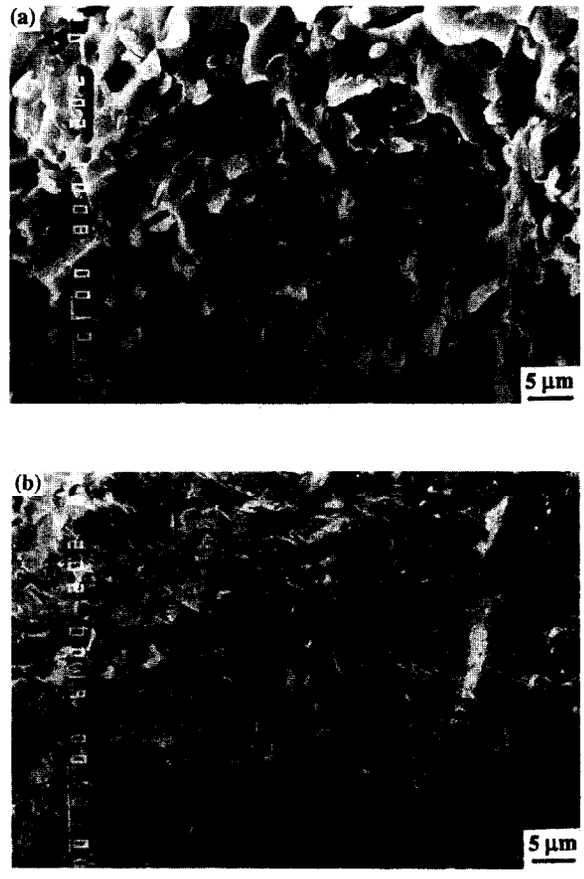

Fig. 12. SEM observation of fracture surface. (a) Al_2O_3 platelet reinforced sialon composite showing debonding. (b) Monolithic X-sialon showing intragranular fracture.

matrix are thought to be the crucial factors determining the toughening of ceramics. Since the thermal expansion coefficient of Al_2O_3 is much higher than that of X-sialon a high internal stress might be generated by this large thermal expansion mismatch in this system; circumferential compression and radial tension are created in the matrix and the platelet is in tension. In this situation cracks are deflected around the platelets. Interfacial bonding at the alumina–X-sialon interface appears to be sufficiently weak for the cracks to follow the contours of the platelets as can be seen in Fig. 8.

5 Conclusions

X-sialon phase can be toughened by Al_2O_3 platelet additions. Reinforcing Al_2O_3 platelets were not agglomerated and well distributed throughout the matrix. Due to hot-pressing, however the material shows alignment of Al_2O_3 platelets with the basal face normal to the hot-pressing direction.

The mechanical properties of hot-pressed sialon composites reinforced with Al_2O_3 platelets were investigated as a function of Al_2O_3 platelet content. The toughness has been shown to increase from 1·77 MPa · $m^{1/2}$ for pure X-sialon up to 4·16 MPa · $m^{1/2}$ for the composite containing 28 vol.% platelets. For higher platelet additions, toughness increases further but the composition of the matrix shifts to β'-sialon. A Young's modulus of 250 GPa and hardness of 1270 kg/mm^2 were achieved in the X-sialon containing 28 vol.% platelet.

SEM and TEM observations of the crack propagation behaviour, along with the fractography result revealed the evidence of debonding, crack bridging and crack deflection, all contributing to the toughening of X-sialon by Al_2O_3 platelets.

References

1. Jack, K. J., Review: sialons and related nitrogen ceramics. *J. Mater. Sci.*, **11** (1976) 1135–58.
2. Gauckler, L. J., Lukas, H. L. & Petzow, G., Contribution to the phase diagram Si_3N_4–AlN–Al_2O_3–SiO_2. *J. Am. Ceram. Soc.*, **58** (1975) 346.
3. Ekstrom, T. & Nygren, M., Sialon ceramics. *J. Am. Ceram. Soc.*, **75** (1992) 259–76.
4. Vleugels, J., Laoui, T., Vercammen, K., Celis, J. P. & Van Der Biest, O., Chemical interaction between a sialon cutting tool and iron-based alloys. Accepted for publication in *Mater. Sci. Engng.*, **A187** (1994) 177–82.
5. Laoui, T., Vleugels, J., & Van Der Biest, O., Effect of secondary phase on sialon/steel chemical interaction. Accepted for publication in *J. Mater. Sci. Engng.*, **A183** (1994) L19–L21.
6. Zhou, Y., Vleugels, J., Laoui, T. & Van Der Biest, O., Preparation and properties of x-sialon ceramics. *J. Mater. Sci.* (submitted).
7. Vleugels, J., & Van Der Biest, O., unpublished work.
8. Faber, K. T. & Evans, A. G., Crack deflection processes: I, theory. *Acta Metall.*, **31** (1983) 565–76.
9. Claussen, N., Ceramic platelet composites. In *Proc. 11th RISØ Int. Symp. Metallurgy and Materials Science 1990, Structure Ceramics Processing, Microstructure and Properties*, ed. J. J. Bentzen, J. B. Bilde-Sørensen, N. Christiansen, A. Horsewell and B. Ralph. RISØ National Laboratory, Roskide, Denmark, 1990, pp. 1–12.
10. Hanninen, M., Haber, R. A. & Niesz, D. E., Mechanical properties of silicon carbide platelet and particulate reinforced silicon nitride. *Ceram. Trans.*, **19** (1991) 749–56.
11. Ketchion, S. M., Leng-Ward, G. & Lewis, M. H., SiC dispersoid-reinforced Si_3N_4 composites. *Ceram. Trans.*, **19** (1991) 757–64.
12. Fischer III, W. F., Haber, R. A. & Anderson, R. M., Mechanical properties of alumina matrix composites reinforced with silicon carbide platelets and particulate. *Ceram. Trans.*, **19** (1991) 773–80.
13. Becher, P. F., Microstructural design of toughened ceramics. *J. Am. Ceram. Soc.*, **74** (1991) 255–69.
14. Anstis, G. R., Chantikul, P., Lawn, B. R. & Marshall, D. B., A critical evaluation of indentation techniques for measuring fracture toughness: I, direct crack measurements. *J. Am. Ceram. Soc.*, **64** (1981) 533–8.
15. Zangvil, A., Gauckler, L. J. & Ruhle, M., Indexed x-ray diffraction data for the sialon x-phase. *Mater. Sci. Lett.*, **15** (1980) 788–90.
16. Morrell, R., *Handbook of Properties of Technical & Engineering Ceramics*. Her Majestys Stationery Office, London 1985, pp. 95.
17. Hayami, R., Si_3N_4–SiC whisker composite material. *Mater. Sci. Res.*, **20** (1986) 663–74.
18. Bennison, S. J. & Harmer, M. P., Grain-growth kinetics for alumina in the absence of a liquid phase. *J. Am. Ceram. Soc.*, **68** (1985) C-22–C-24.
19. Rödel, J. & Glaeser, A. M., Anisotropy of grain growth in alumina. *J. Am. Ceram. Soc.*, **73** (1990) 3392–401.
20. Kaysser, W. A. & Sprissler, M., Effect of a liquid phase on the morphology of grain growth in alumina. *J. Am. Ceram. Soc.*, **70** (1987) 339–43.
21. Takatori, K., Pressureless sintering and mechanical properties of alumina–sialon composites. *J. Mater. Sci.*, **26** (1991) 4484–90.
22. Davidge, R. W., *Mechanical Behaviour of Ceramics*, ed. R. W. Cahn, M. W. Thompson and L. M. Ward. Cambridge Unversity Press, 1979, pp. 24.
23. Chos, Y. S. & Green, D. J., Silicon carbide platelet/alumia composites: II, mechanical properties. *J. Am. Ceram. Soc.*, (1993) 1452–8.
24. Sakai, K., Matsuhiro, K. & Furuse, Y., Mechanical properties of SiC platelet reinforced ceramic composites. *Ceram. Trans.*, **19** (1991) 765–72.
25. Yamai, I. & Ota, T., Thermal expansion of sialon. *Adv. Ceramic Mater.*, **2** (1987) 784–8.
26. Gauckler, L. J., Prietzel, S., Bodemer, G. & Petzow, G., Some properties of β-$Si_{6-x}Al_xO_xN_{8-x}$. *Nitrogen Ceramics*, ed. F. L. Riley. Noordhoff, Leyden, Netherlands, 1977, pp. 529–37.